3D Assessment of Irreversible Electroporation Treatments in Vegetal Models

Banús Cobo, Jaume

Curs 2014-2015

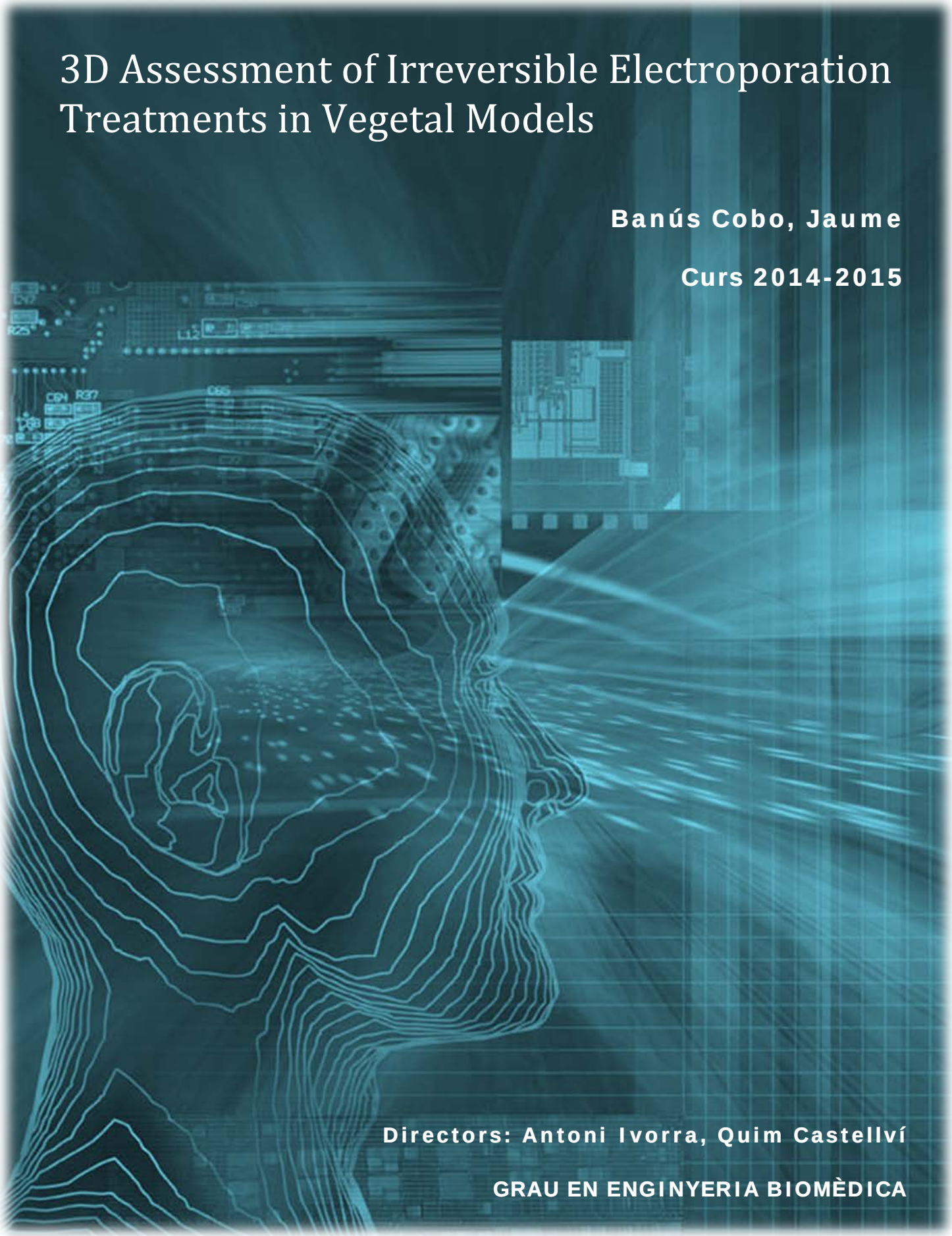

Directors: Antoni Ivorra, Quim Castellví

GRAU EN ENGINYERIA BIOMÈDICA

upf. Universitat Pompeu Fabra Barcelona
Escola Superior Politècnica

Treball de Fi de Grau

Universitat Pompeu Fabra Barcelona

3D Assessment of Irreversible Electroporation Treatments in Vegetal Models

Final Degree Thesis

Jaume Banús Cobo

Supervisors:

Antoni Ivorra

Quim Castellví

Table of Contents

Summary

In the last years irreversible electroporation techniques (IRE) has started to gain importance exponentially in the medicine field, from being considered as an undesirable side-effect of reversible electroporation treatments to being considered nowadays as a viable treatment against cancer by its right own.

IRE treatments are based in electroporation, electrical pulses are delivered to damage the cell membranes and cause the cell death. It has numerous advantages compared with other ablation techniques since is a non-thermal ablation, thus, the tissue scaffold is spared when the treatment is applied. Is possible to predict the extension and shape of the treatment by means of mathematical simulations, the models used to predict that have been experimentally refined.

We present an improved method to evaluate in three-dimensions the results of IRE using vegetal models. The technique consists on using a dye solution to enhance the IRE area in sliced potato tubers. After slice digitalization, the electroporated area was automatically identified and the resulting treated volume was calculated. In addition, a threedimensional reconstruction of both healthy tissue and IRE volume was generated. The proposed evaluation technique was used to assess different pulse protocols outcomes. Finally, numerical simulations had been carried out to compare the numerical predictions to the experimental observations. The obtained results shows a clearly match between experimental and simulated volumes confirming the reliability of the method proposed.

1. Introduction

1.1. Definition

Electroporation is a phenomenon in which permeability of cell membranes is modified due the applications of short high-voltage pulses. This modifies the ion flow of the membrane and allows the pass of molecules which previously can't travel through the membrane.

Although there are a lot of parameters which affect the electroporation outcome the main one is the local strength of the electric field. If the local electric field achieves a certain threshold we talk about reversible electroporation (RE), here the cell resale its membrane once the pulses finished and recovers its normal activity. However, if a second higher threshold is achieved we talk about irreversible electroporation (IRE) the cell membrane is unable to resale its membrane this leads to a permanent loss of homeostasis in the cell which generates high stress levels in it and eventually leads cell to dead. In this project, we will focus in the analysis of IRE protocols.

IRE can be used to directly kill cancer cells, but until a few years ago in medicine was considered as an undesirable side effect of RE treatments used electochemotherapy (ECT), now is started to be considered as a viable treatment by its own right. Recently has emerged as an alternative to other thermal ablation techniques since affects only the cell membrane and no

other structures in the tissue, the structure of bile ducts, blood vessels, and connective tissues remains intact in IRE protocols. [1]

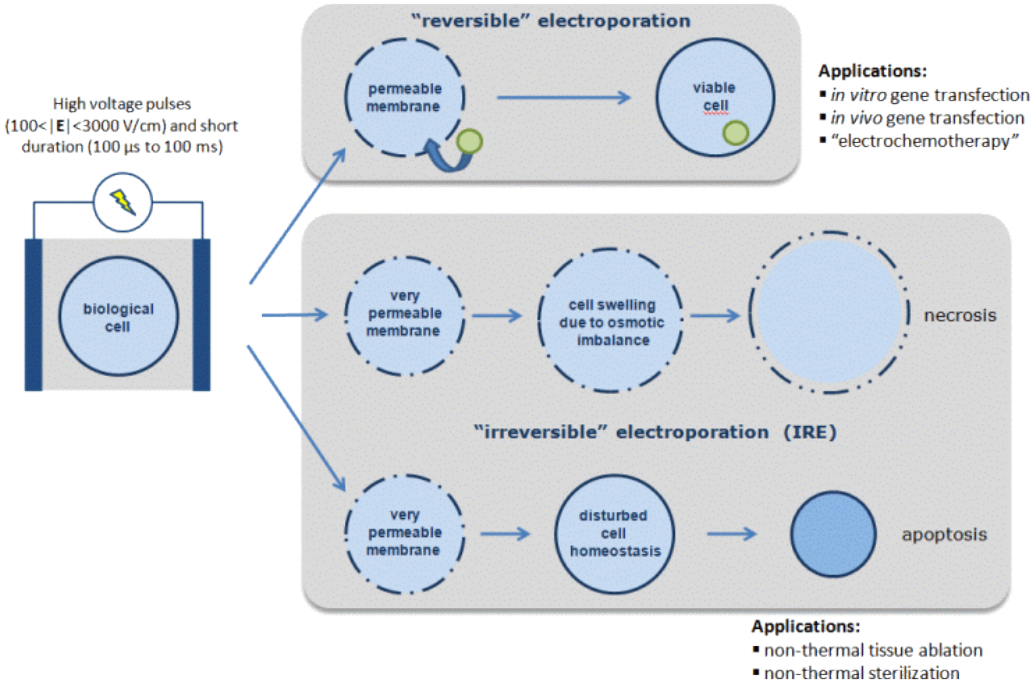

Figure 1: Illustration in which difference between reversible and irreversible electroporation is observed. Image from BERG website.

1.2. Molecular mechanism

The molecular mechanism involved in the electroporation is not fully understood yet. But in over the past years several studies has been carried out in order to understand the physiological changes which happen in the cell when electroporation occurs.

Theoretical modeling and experimental data on black lipid membranes suggest the creation of aqueous pathways, a bioelectrochemical process; other descriptions suggest a more complex process where mostly the membrane–solution interface is altered. But there is general agreement in the literature, that nanometer-sized metastable structural defects or "pores" are created [2], and in [3] pore-like structures of nanometer-size had been observed by means of scanning electron microscopy (SEM).

The formation of the pores is a stochastic process, which is based on thermodynamic considerations, the formation of aqueous pores is initiated by the penetration of columns of water molecules into the lipid bilayer of the memrbane. Under the electric field, water dipoles orient and form almost single molecule-thick columns which penetrate the layer of the lipid tails. Then phospholipid heads move also towards the interior of the membrane and columns rapidly enlarge to form hydrophilic conductive large pores [4]. (Figure 2)

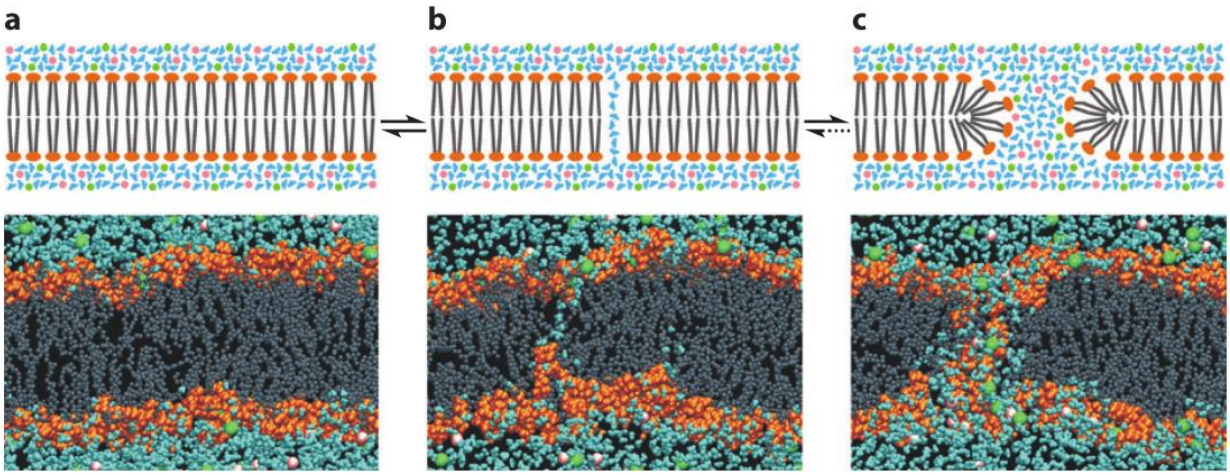

Figure 2: An idealized molecular-level scheme (top) and an atomic-level molecular dynamics simulation (bottom) of electroporation with the electric field perpendicular to the bilayer plane. (a) The intact bilayer. (b)Water molecules start penetrating the bilayer, forming a water wire. (c) The lipids adjacent to the water wire start reorienting toward the wire with their polar head groups, stabilizing the pore and allowing more water, as well as other polar molecules and ions, to enter. [4]

1.3. Treatment plan and imaging

Treatment planning is essential for successful electroporation. Efficient cell membrane electroporation depends on establishing a sufficiently high electric field locally (i.e., in the target tissue).

The ultimate goal of treatment planning is, therefore, to model electrode position and number; electric field amplitude; and pulse duration, number, and frequency to non-thermally ablate only the targeted tissue.

The current treatment planning models focus on (a) electrode position, to cover the target tissue by electric fields and spare non-target tissue; (b) electric field protocol optimization, to delineate the thermal damage and avoid irreversible electroporation in the case of GET or ECT; and (c) integration of mathematically derived treatment planning with diagnostic imaging. [4] An example of a treatment plan used in ECT is shown in Figure 3.

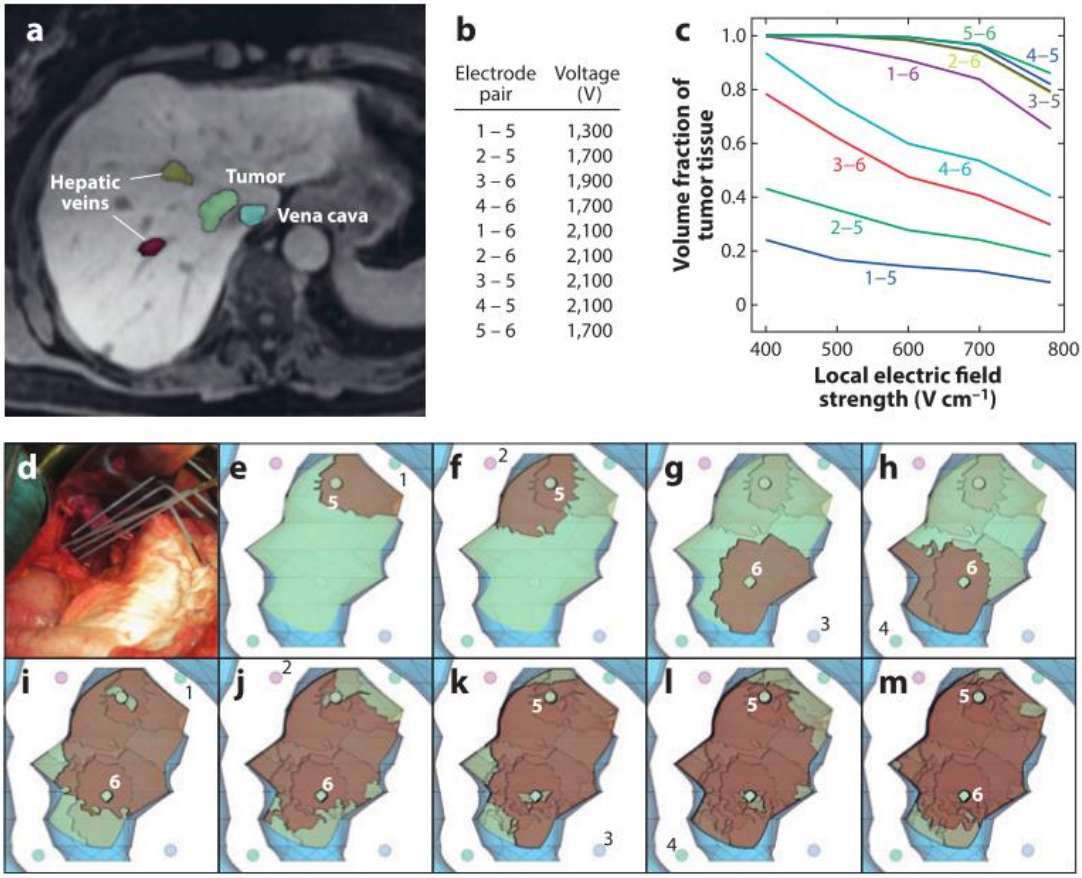

Figure 3: Treatment plan used in a case of colorectal liver metastasis.[4]

The basic workflow followed in a treatment plan can be summarized in:

1. Process patient images acquired with CT or MRI.
2. Verify and correct segmentation and obtain 3D model of the ROI.
3. Select electrode layout
4. Optimize the electric field

In order to be able to select the electrode layout and optimize the electric field to treat the whole tumor and spare as much healthy tissue as possible is necessary take into account the non-linear conductivity changes produced in the tissue once the electric field is applied. Then is necessary the use of numerical models to predict the local field intensity in the tissue. Statics and dynamical models, like asymmetrical sigmoidal curves, has been used to model the conductivity and is has been seen that dynamical models are able to predict the affected zone more accurately. [5]

Towhidi et al. [6] reports an experimental study in which multiple cells exhibit different electroporation thresholds depending on their sizes, shapes and orientations. Besides the intercellular distances will also play a significant role. That is, the separation between cells will modulate the transmembrane potential induced by the external macroscopic field [7], making the electroporation thresholds particular for each tissue. But conductivity changes not only

depends on tissue properties also depends on stimulation parameters like amplitude, duration, number, shape and frequency of the delivered electric pulses. It was also shown that the dependency on voltage, duration, and number of pulses is complex [8], [9], but the local primary parameter affecting the degree of electroporation is the local field strength [10].

Each cell has a different threshold, thus we can imagine each cell as a switch, then we can approximate the conductivity of a tissue as a convolution of different step functions with different thresholds, and we obtain a sigmoid curve. For a particular tissue is possible to experimentally determine its conductivity and fit it to the most appropriate numerical model, as pointed out before an asymmetrical sigmoid curve theoretically should be a good approximation [10]. This numerical model will be used in finite element simulations (FEM) to simulate the conductivity of the tissue in function of the local electric field.

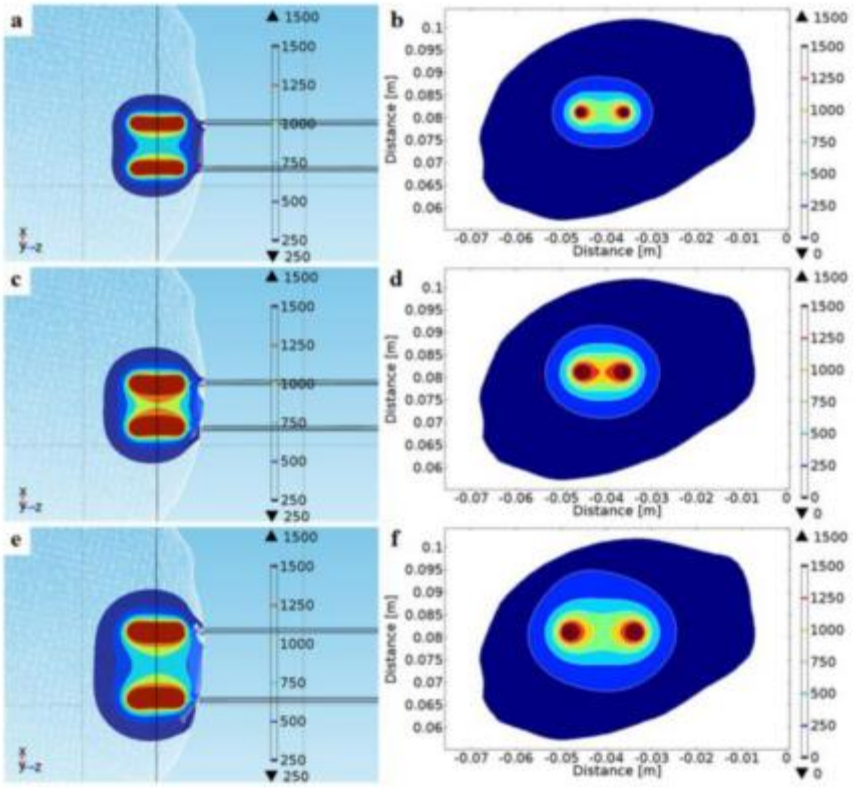

Figure 4: Numerical model electric field isocontours (V/cm). [5]

The 3D computational model used in FEM is obtained from the medical images of the patient. Combining FEM with numerical models is possible to calculate the electric field and temperature distributions over the tissue and so the shape and extension of a particular treatment (Figure 4). It is assumed that the tissue region is affected by IRE once the electric field magnitude is higher than a certain threshold value, which is determined experimentally by the correlation between numerical models and simulations [11]. FEM is used instead of analytical methods due in clinical practice treated geometries are not trivial. The key idea of the FEM is the decomposition of the geometry into small simple elements (i.e. the mesh of elements) in which it is possible to

solve differential equations related to the phenomenon under study. Boundary conditions impose the constraints that allow the method to generate a single approximate solution for the complete geometry.

The optimization of the electrodes position and the applied voltages between them is usually carried out by a genetic algorithm. The goal as said before is to treat the whole ROI and spare as much healthy tissue as possible. For this the algorithm have as main constrains, the number of electrodes, the technical specifications of the pulse generator and the increase of temperature. Then using FEM and the chose numerical model the genetic algorithm will rank the approaches with fitness dependent on the non-treated tumor volume and the affected healthy tissue. [12]

Once the treatment is planned to precisely insert the electrodes the introduction of the electrodes is guided by means of US or CT. And the electroporation of the area can be monitored at real time by means of electrical impedance tomography (EIT) [13] or US [14]. Also is necessary to synchronize the pulses administration during IRE with the refractory period of the cardiac cycle using ECG, to avoid possible cardiac arrhythmias [15], and is necessary anesthesia since muscular contractions are produced due electric pulses which produce pain in the patient [16]. Arena et al [37] recently developed a pulse protocol to try to minimize muscle contraction during treatments known as high-frequency irreversible electroporation (H-FIRE), which utilizes high frequency, bipolar bursts to eliminate muscle contraction, without sacrificing the efficiency of cell death due to non-thermal electroporation. The clinical application of H-FIRE may eventually eliminate the need to administer neuromuscular agents during the IRE procedure. After the treatment a follow up of some months is necessary, by means of CT, MRI, US or PET [17].

Nevertheless, accurate matches between mathematically predicted and real ablated area are seldom reported [18], [19] and a certain miss-match is commonly observed. This discrepancy could be produced by multiple factors such as tissue fibers, tissue organization, cell orientation or cell shape.

The main problems nowadays is the lack of reported conductivity values of tissues in literature, and that the experimental threshold is valid if the treatment parameters (duration, number of pulses, frequency, shape of pulse) are the same and the only changes are distance between needle electrodes and voltage applied between them. Thus is necessary to carry out more studies to assess the effect of other pulse parameters besides voltage and be able to characterize its behavior in new treatment plans.

1.5. Vegetal models

Then although IRE treatments protocols have been extensively studied, further studies are required to improve the prediction methods and the IRE protocols. However those studies could involve a high number of animals, histological observations and its associated costs. With the

aim of explore the electroporation outcomes with an inexpensive model and to follow the replacement concept of the 3Rs, alternative models had been proposed [10], [20].

The potato is a good model often used to assess the IRE outcomes. Those tubers are commonly employed since the tissue affected by IRE will become darker in a couple of hours. Furthermore potato shows a quite isotropic tissue structure which simplifies the studies. This technique of observation has been employed in multiple occasions to study the relation between applied protocols and IRE outcomes [21] and in order to compare predicted outcomes with the real ones [10]. The blackening process is attributed to an accelerated oxidation produced by enzymes released during the cell lysis [22]. It implies that parts of the potato closest to the surface, which are in direct contact with the air, are darker than inner parts despite being equally affected by IRE. In addition, the treatment outcomes are commonly observed about 12 hours after the pulse application, producing a desiccation of the sample which could mean a change of the morphology and, therefore, an error of outcomes measurements.

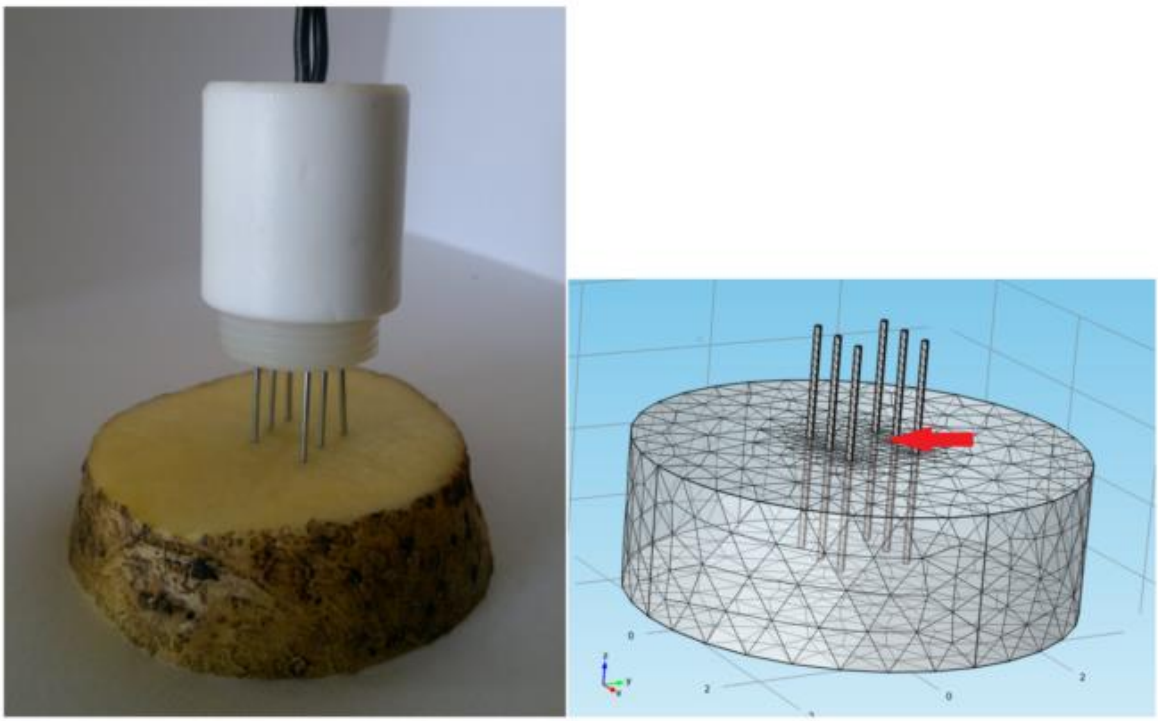

Figure 5: In vitro and in silico models. [21]

1.6. Motivation

As introduced systematically studies or IRE protocols are needed to better understand the effect of the different pulse parameters (duration, number of pulses, frequency, shape, voltage) and improve the existing numerical methods in order to obtain better predictions which can help to improve treatment plans.

Also as pointed out a good choice to carry out this systematically studies can be vegetal models such potatoes, but we think that the blackening process is not a reliable marker, so in this project we purposed the use of a common food colorant to enhance the irreversibly electroporated areas. Potatoes have a high compact tissue structure with a high density of cells, when IRE occurs, the cell death entail a turgor pressure loss [23] changing the mechanical properties of the tissue.

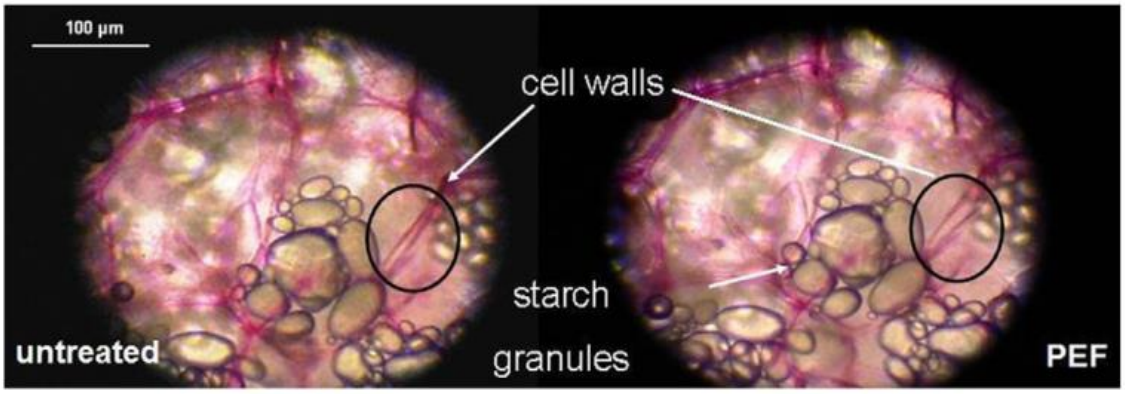

Figure 6: Untreated and PEF treated potato tissue stained with ruthenium red. [24]

In Figure 6 is appreciable the change in cell walls after the application of the electric pulses. The morphological changes in the tissue structure produce a loss of turgidity in the electroporated areas which produce an increase on tissue permeability to liquid. This effect is proposed in [24] to dye the treated areas, as we will do in our project.

This improved observation technique allows to observe fine slices regardless the desiccation effect. Thus, it is possible to observe the inner parts of the potatoes to assess the tridimensional outcomes of applied electroporation protocol.

The goal is to analyze different electroporation protocols by means of 3D reconstruction, to see which variable has more impact in them, and so be able to choose a protocol with a minimum variability when a patient is treated.

2. State-of-the-art

2.1. History of IRE and its role in medicine nowadays

The first observation of electroporation was reported in 1958 by Stampfli [25]. He noticed that on electrically stimulated membranes its dielectric properties change and this effect could be reversible under certain circumstances. This phenomenon was described as “membrane breakdown,” which in more recent work is considered to be an increase of membrane conductance or permeability. [2]

IRE research has advanced in a parallel way in the field of biomedicine and in the area of food processing, either using the cell membrane lysis produced by electroporation by extract the

contents of microorganisms or by taking advantage of its bactericidal effect in treatment of fluids.

In 1967 Sale and Hamilton [26]–[28] studied the effect of strong DC pulses on microorganisms. They reported the non-thermal killing effects of these pulses and observed that leakage of intracellular ions and molecules occurs immediately after the application of the electric field pulses. With this they elucidated that the mechanism by which the electric field pulses leads cells to dead is an irreversible loss of the membrane semipermeable function.

However by then IRE was not taking into account in biomedicine field, and the big advances were made in reversible electroporation. In 1982 Neumann et al. [29] were the first ones to facilitate gene transfer into cells by means of reversible electroporation. This created a powerful method for gene transfection that has been used in microbiology labs for more than 30 years, and 7 years ago reached the first clinical trial [30]. In the early 90s many studies demonstrated the utility of electroporation in molecular biology, mainly as a method to introduce foreign molecules into living cells when electroporation is reversible. Mir pioneered the use of in vivo electroporation for the introduction of chemotherapy drugs in solid tumors [31] including the first clinical trial [32] and now the pairing of electroporation and chemotheapeutic drug quickly gained popularity and exists as an independent treatment termed electrochemotherapy (ECT) which is in clinical practice [33]. The reported objective response rates of ECT range from 72% to 100%, and is one of the most well-established clinical applications of electroporation today.[2]

Until recently, irreversible disruption of cell-membrane integrity by IRE had only found a practical use in microbial inactivation in the food industry. In medical applications irreversible electroporation was considered as an undesirable side-effect of reversible electroporation until Davalos et al. [34] in 2005 demonstrated that IRE was able to kill cancer cells in a similar way to more traditional ablation therapies such as radiofrequency (RF) heating or cryosurgery but without produce thermal damage in the surrounding tissue.

Further studies have confirmed the absence of considerably thermal damage and demonstrated some additional advantages that IRE has over other thermal and chemical ablation techniques. 1) IRE is a non-thermal physical ablation modality. 2) Avoid influence of local blood perfusion on treatment outcome (i.e., no blood sink or source to heat transfer). 3) Delineation between treated and untreated tissue after IRE is very sharp. 4) IRE affects only cell membranes and leaves extracellular structures intact, is possible to preserve microvasculature. 5) IRE allows rapid regeneration of ablated tissue without scar formation. [17]

These advantages quickly triggered widespread interest from the scientific community leading to many studies both in vitro and in vivo. Further, a wide variety of cell, organ, and animal models have been used to characterize the destructive potential of IRE for different cancer types. [2] Among them we can highlight the first in vivo use of IRE in animal studies reported by Edd et al. [35] in 2006, and the first in vivo use reported in humans by Pech et al. [36] in 2010.

These studies have provided valuable experimental results and treatment planning protocols (IRE threshold, pulse parameters, etc.) including electrode delivery (electrode design, placement, intraoperative imaging methods, etc.), injury evaluation (methods and timing), and treatment efficacy.

2.2 Clinical treatment plans in IRE

Clinical procedures like IRE require medical devices specifically designed to accomplish strict conditions of performance and safety. Nowadays there is one commercial IRE system (NanoKnife; AngioDynamics, Queensbury, NY,USA) its design was reported in 2007 by Bertacchini et al. [15] it was the first IRE system approved for clinical use.

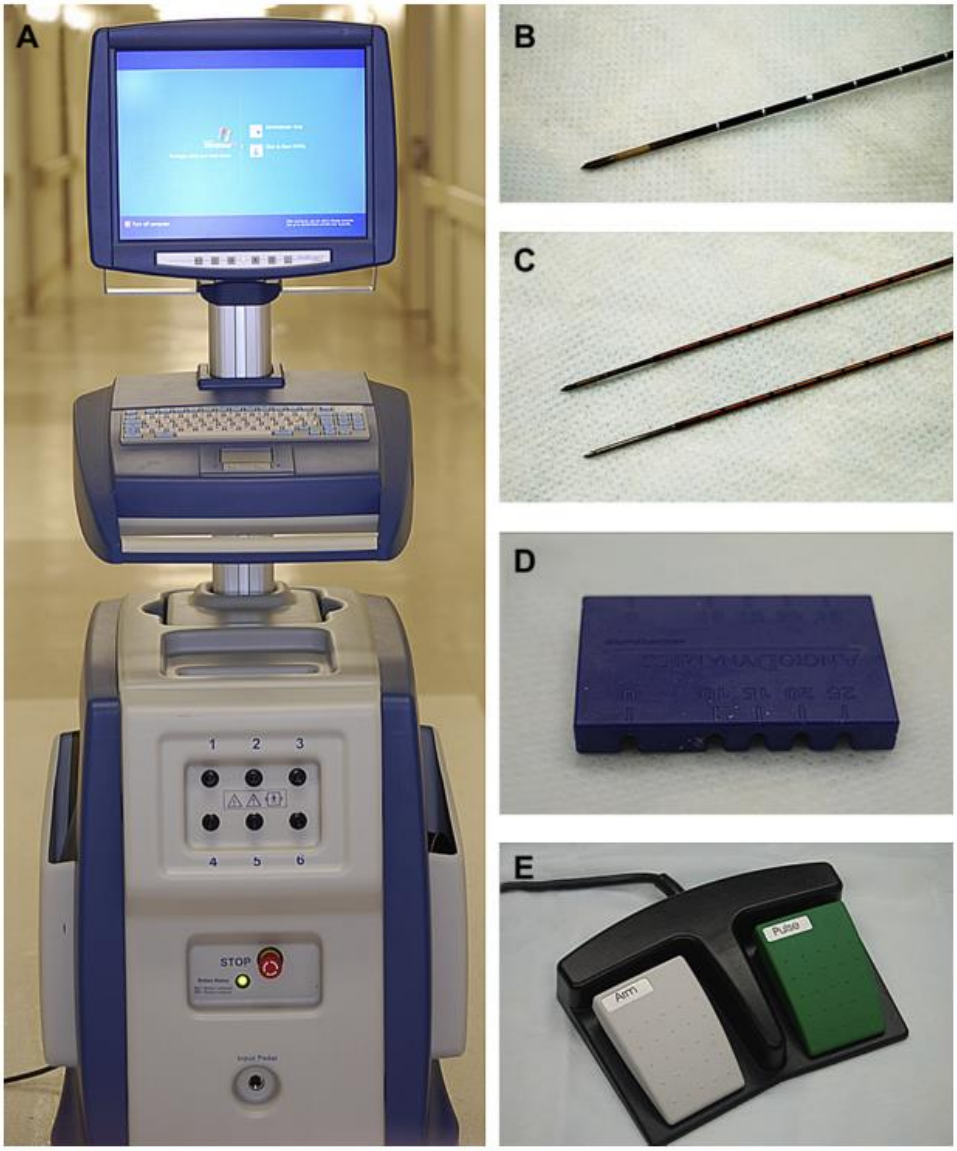

Figure 7: Current IRE system. (A) IRE generator from AngioDynamics Inc. (B) 16G Bipolar IRE probe. (C) 19G monopolar IRE probes. (D) Monopolar IRE probe spacer. (E) IRE generator pedal. IRE, irreversible electroporation. [17]

The system consist of two main components: an IRE generator, which can deliver between 100-3000V in 90-100 pulses, and up to six electrode probes of 15cm length and 16-19 gauge in diameter.

The software of the console follows the numerical methods presented in[37] and [34].They use a single pulse of the length of the whole pulses and although nowadays there are numerical simulations which use specific electrical properties of the tissues, the increase of electrical conductivity due electroporation is not taken into account. [38]

Besides NanoKnife console provides 2D images of the cross-sectional ablated zone perpendicular to the needle direction. To generate a 3D volume from here is necessary to use some image software which takes the whole 2D ablation cross-section areas along the length of the needles and stack them.

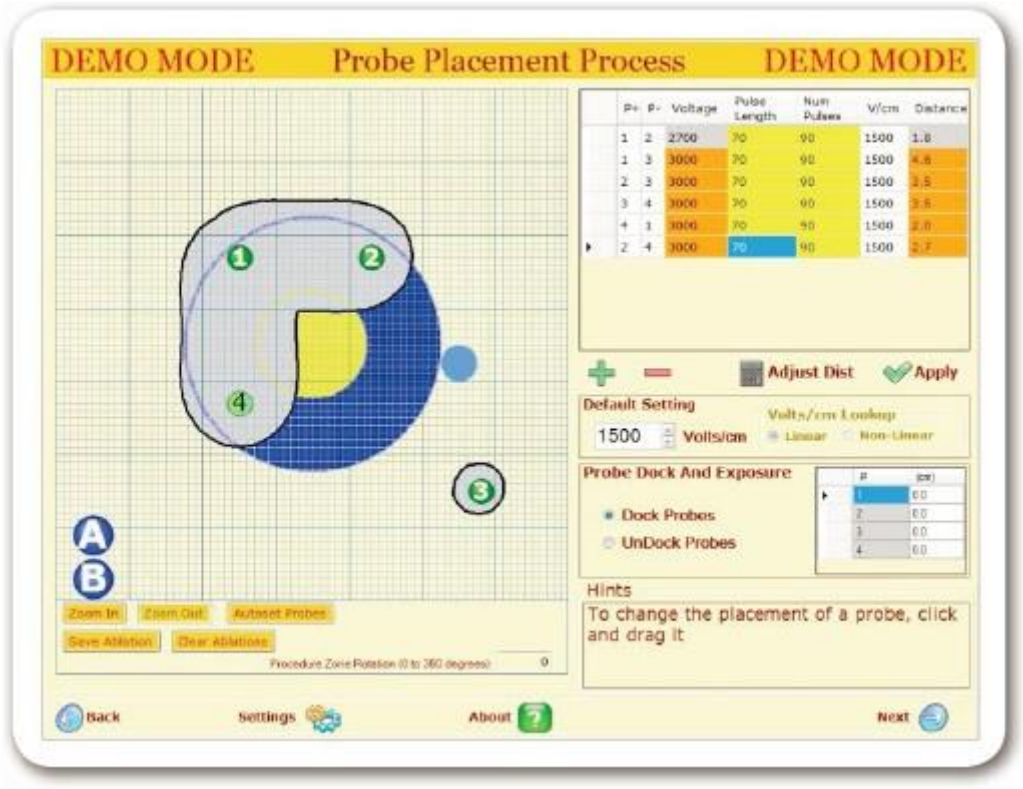

Figure 8: Treatment Planning Software version 2.2.0 – Treatment Planning Screen image from AngioDynamics website.

3. Methods

A total amount of 60 potatoes (Solanum tuberosum, Monalisa) were used in the whole experiments. All potatoes were bought from the same local supermarket. Each potato had treated with a single treatment applied by means of needle shape electrodes.

3.1. Electroporation setup

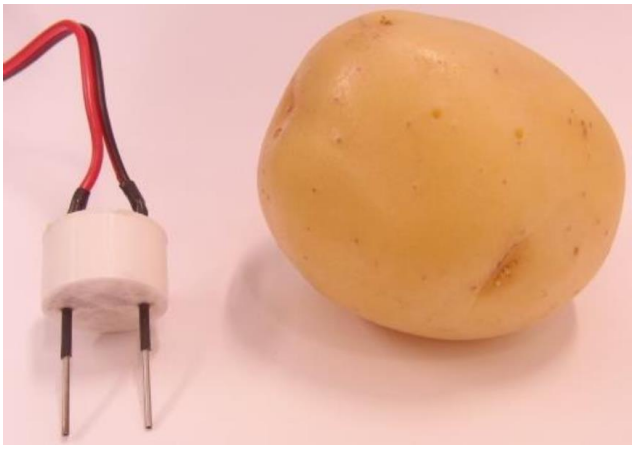

Figure 9: Two needle electrodes used during the experiment and a potato with holes in the peel produced by the insertion of the electrodes.

The electrodes consist on two parallel stainless steel cylinders of 1.27 mm diameter separated 15 mm mounted on an ABS plastic holder. These electrodes were inserted, through the peel, reaching the dip part of the potatoes where IRE treatment was applied. In order to avoid boundary effects at the surface, the proximal part of the electrodes was isolated leaving an active part of 15 mm.

That setup was used to evaluate the influence of duration, magnitude and number of pulses over the IRE outcomes. The experiments were carried out tuning each one of those parameters independently of the others. A summary of the applied protocols can be seen in table 1.

	Voltage [V]	**# Pulses**	**Pulse duration [us]**	**# Samples**
Voltage	250	10	100	4
	500	10	100	4
	750	10	100	4
	1000	10	100	4
	1250	10	100	4
Pulses	500	1	100	4
	500	3	100	4
	500	10	100	4
	500	30	100	4
	500	100	100	4
Pulse duration	500	10	10	4
	500	10	30	4
	500	10	100	4
	500	10	300	4
	500	10	1000	4

Table 1: Assessed electroporation protocols.

All these protocols in both studies were delivered at 1Hz by means of a custom made generator able to deliver the specified pulse protocol.

3.2. Sample preparation

Our approach to obtain proper potato slices to carry out a good segmentation, and thus a 3D reconstruction, is the following: First apply the specific electroporation protocol to the potato and after some time cut it into slices, following bath those slices into a dyeing solution and after another amount of time remove them and immersing them into a distilled water solution to wash them and thus enhance the contrast.

To obtain a systematic protocol for that approach we needed to determine: elapsed time between protocol application and slices cut, time remaining of the slices into the dyeing solution, and necessary amount of ions to make both dyeing solution and washing solution isotonic and avoid the swelling or decrease of potato slices.

3.2.1. Osmolarity assessment

The dye (Wilton Ice Colorant –Sky Blue) was diluted into distilled water at a ratio of 0.5ml of colorant for each 100ml of distilled water.

To find the necessary amount of ions which we had to add to reach osmotic equilibrium between the potato slices and the solution we performed the following experiment.

We prepared different samples of the same solution and added different amounts of NaCl to each one. We left the potato slices one hour into the solutions and used one slice as control, which remained an hour into a petri dish. In table 2 is visible the amounts of NaCl used in %.

We scanned the potato slices after and before the bath and then used MATLAB (The MathWorks, Inc.USA) to calculate the difference between the areas before and after. Then we used the solution which gave us the minimum difference to dye all the samples of our experiments.

Saline	1.2	1.3	1.4	1.5	1.6	-	-
Dye Solution	0.8	0.9	1	1.1	1.2	1.3	1.4

Table 2 : NaCl % concentrations used to assess the osmolarity of both solutions.

As done with the dye solution to find an osmotic equilibrium for the distilled water used to wash the slices we used the same experiment. The experiment setup can be observed in Figure 10.

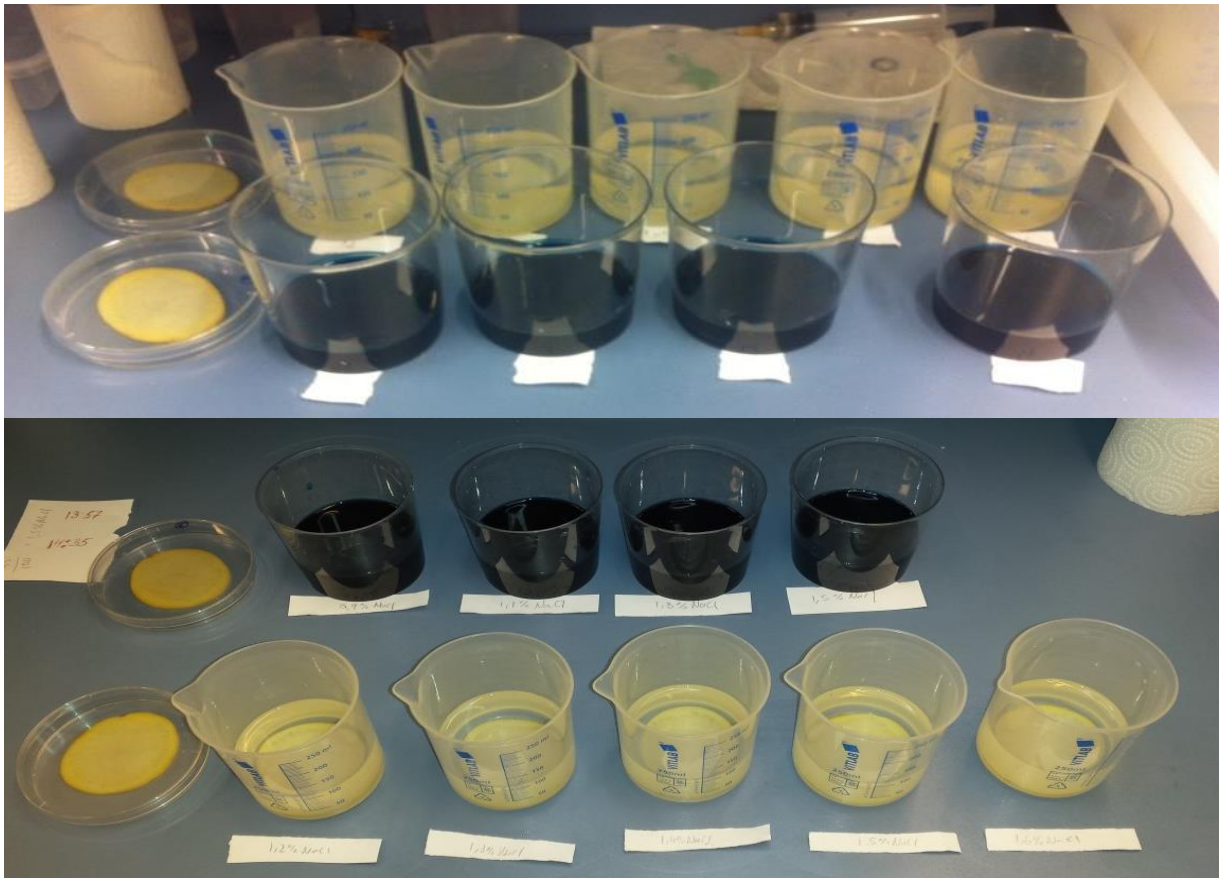

Figure 10: Setup of the experiments we carried out to assess the osmolarity. Notice in the left side of both images the control slices inside petri dishes.

3.2.2. Elapsing time before dyeing bath

Numerous studies have reported the "delay" of injury development after electroporation [2], since the effect of the electroporation is not immediate is necessary to wait a minimum time to achieve enough tissue damage which allows dye to diffuse through the whole ablated area. Thus, we needed to determine the minimum elapsed time between the application of the IRE treatment and the immersion into the dyeing solution.

We wanted to find the minimum necessary time because if we wait too much the black began to appear with the corresponding desiccation and morphological changes, even some holes are produced due the necrosis of the cells if we wait too much, as can be seen in Figure 11, and these facts are undesirable because can affect the algorithm of segmentation and 3D reconstruction.

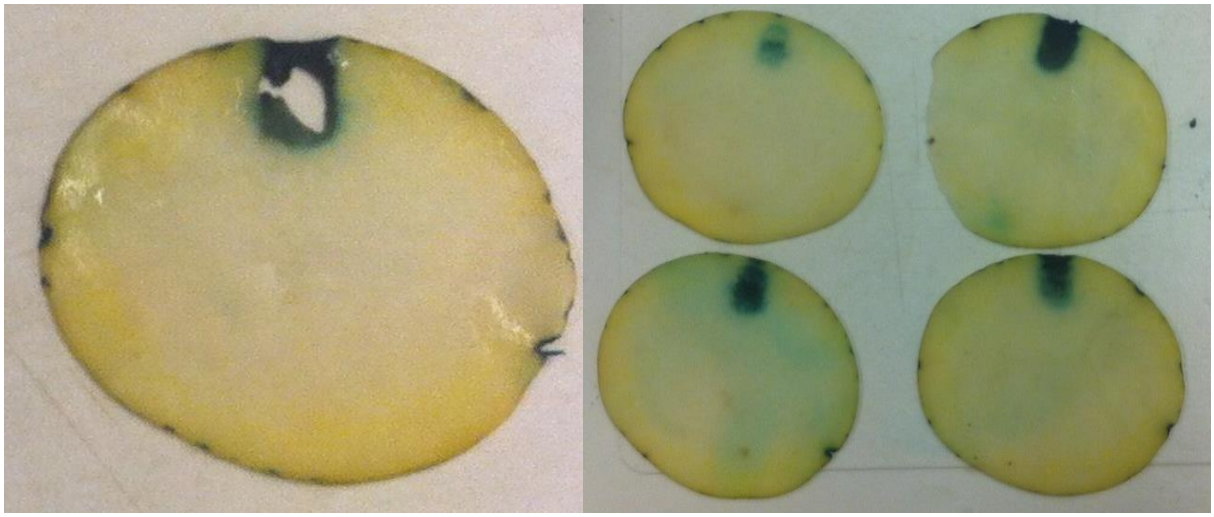

Figure 11: On the left side a potato slice with a hole due necrosis. On the right side potato slices in which black is observable.

To determine this time we performed an experiment consisting into apply the same electroporation protocol and wait different times before apply the dye solution, during the same time always, and after that we determined the dyed area. The dying solution was applied during 24 hours to be sure to dye the whole area in each case. The summary of the experiment can be seen in table 3.

Elapsed time	0	1	3	6	24
Dyeing time	24	24	24	24	24

Table 3: Elapsing time determination experiment.

Once the treated area started to become more or less constant we looked for the minimum time in which that happens and selected it as hour elapsing time.

3.2.3. Dyeing time

As we did for the elapsing time we determined the minimum dyeing time necessary to dye the whole affected area by the IRE. To that we applied the same electroporation protocol and waited enough time to be sure to be able to dye the whole treated area. After that we applied the dye solution for various times and estimated later the dyed area in each test.

Elapsed time	**24**	**24**	**24**	**24**	**24**
Dyeing time	1	3	6	12	24

Table 4: Dyeing time experiment.

As did with the waiting time once the treated area started to become more or less constant we looked for the minimum time in which that happens.

3.3. Segmentation and reconstruction

Each slice was scanned by means of a commercial desktop scanner at 600 dpi resolution, once digitalized the images were processed using MATLAB (The MathWorks, Inc.USA), to obtain first the segmentation and later the 3D reconstruction.

3.3.1. Volume accuracy

Our first goal was determine which accuracy we were able to achieve in the volume reconstruction. Thus, firstly we calculated some potato volumes, to do that we filled a metric container with distilled water and then the potato was submerged into them and observed the raise of water. We considered the raise produced in the metric as the volume of the potato.

Then we sliced the potato and segment it into slices, the slices were scanned and digitalized. The images were processed with MATLAB and once we have the binary mask of the potato slices we calculated the number of white pixels in the image and which fraction of the total amount of pixels represented. Since we knew the total area of the image, a DIN-A4 sheet, we were able to calculate the total area of the potato slices by relating it with the fraction of white pixels. To obtain the volume we used the mean width slice, which was obtained experimentally measuring the total height of the stack of potato slices and dividing it by the number of slices.

After that we compared the obtained volume with the reconstructed and found that were able to achieve an accuracy of 95.90%.

Since the accuracy was high enough, in order to simplify the procedure from now on the mean width slice was calculated from the total volume of the potato. To achieve that, we calculated the density of our potato type, repeating several times the water experiment and weighting the potatoes before, thus we obtained the density and we were able to calculate the mean width slice knowing previously the weight of the potato and the area of the slices.

3.3.2. Segmentation

Since a lot of potatoes were used to carry out the studies we developed a MATLAB graphical interface (Figure 12), in which we were able to load the original images, obtain the necessary binary masks and perform the 3D reconstructions of both the whole potatoes their respective electroproated areas.

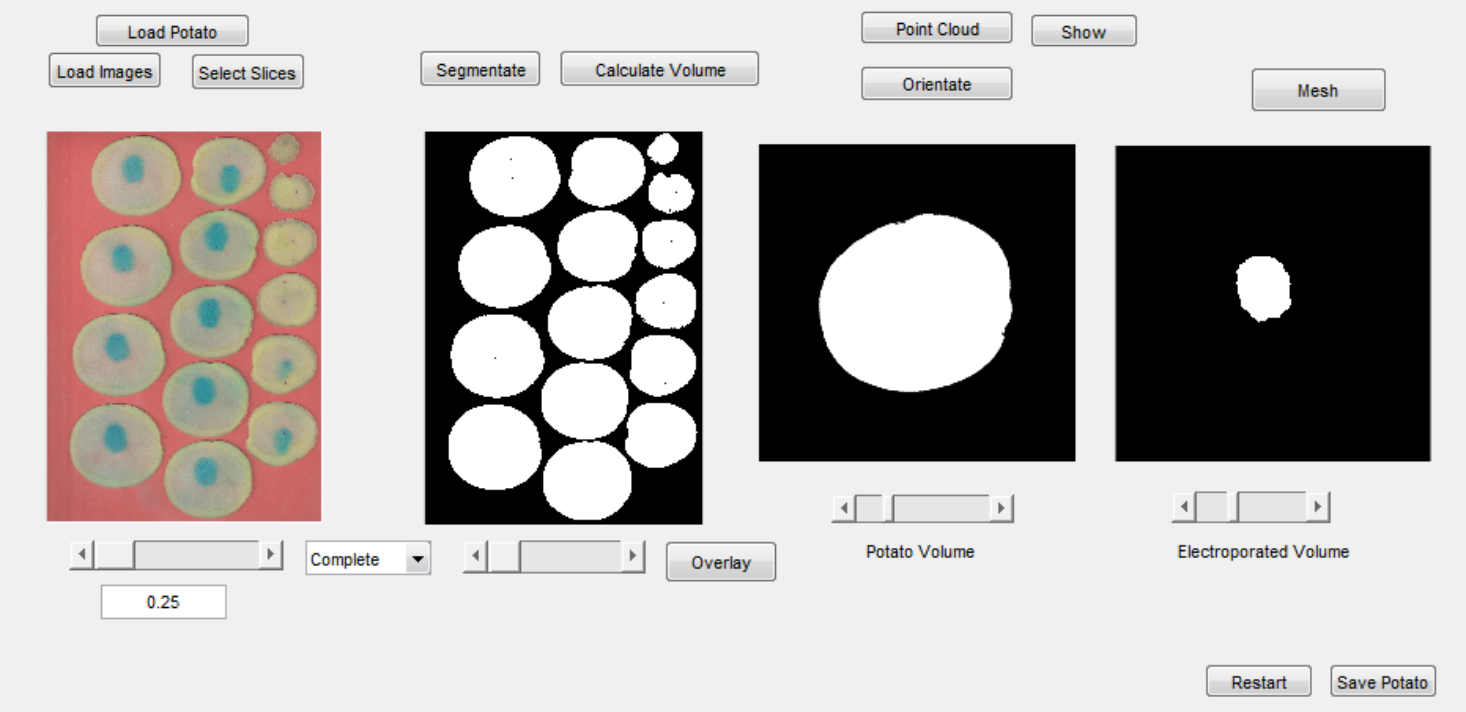

Figure 122: Interface of the MATLAB GUI used to speed up the segmentation and reconstruction of the potato.

To obtain the binary mask of the whole potato the background was removed from the image using K-Means algorithm, and to obtain the mask of the electroporated area the whole RGB image was transformed into YCbCr color space and Otsu's method was used to determine the proper color threshold.

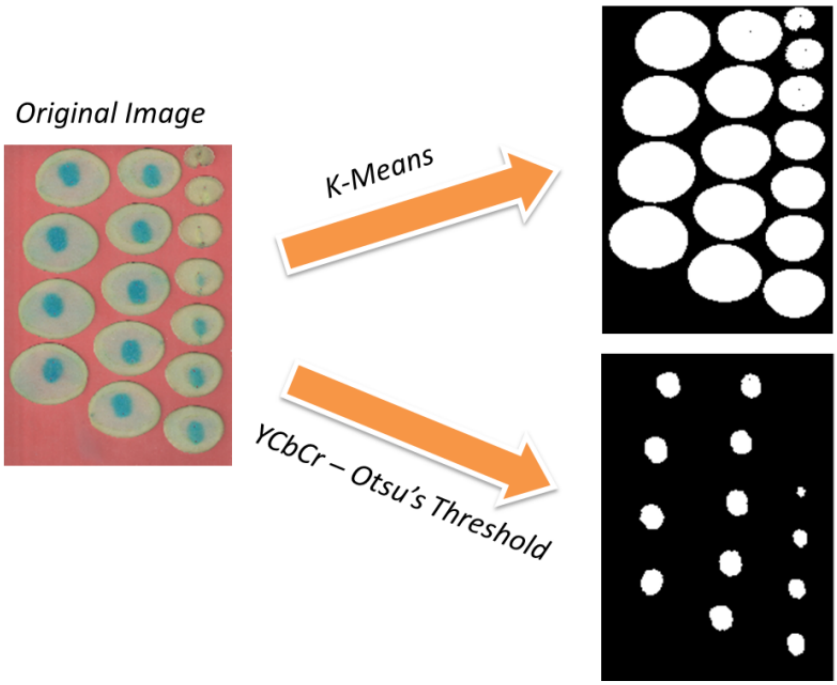

Figure 13: Schematic of how to obtain binary masks from the original image.

Once the binary masks of the whole images have been obtained the goal is to take each binary mask of each slice and create a 3D stack to reconstruct the potato and the electroporated area. To do this first of all we calculated the minim image size to allocate the biggest slice, in order to reduce the computational cost of the reconstruction.

Then we took the whole images with the entire binary slices mask and selected one slice at time, calculated its mass center and the necessary shift to move it from its initial position to the center of the image. Following the corresponding electroporated mask (if exist) is subtracted from the whole slice mask, and the resulting mask is shifted to the center using the previously calculated displacement. This allows to have both, the slice and its electroporated area relocated at the center of the image and with electroporated area maintaining its relative position with respect to the slice. Finally the image is cutted to have the calculated size of the stack.

The 3D stacks of the whole potatoes were obtained by filling each slice of the stacks. And the 3D stacks of the electroporated areas were obtained by doing the inverse of the slices followed by a clear border operation.

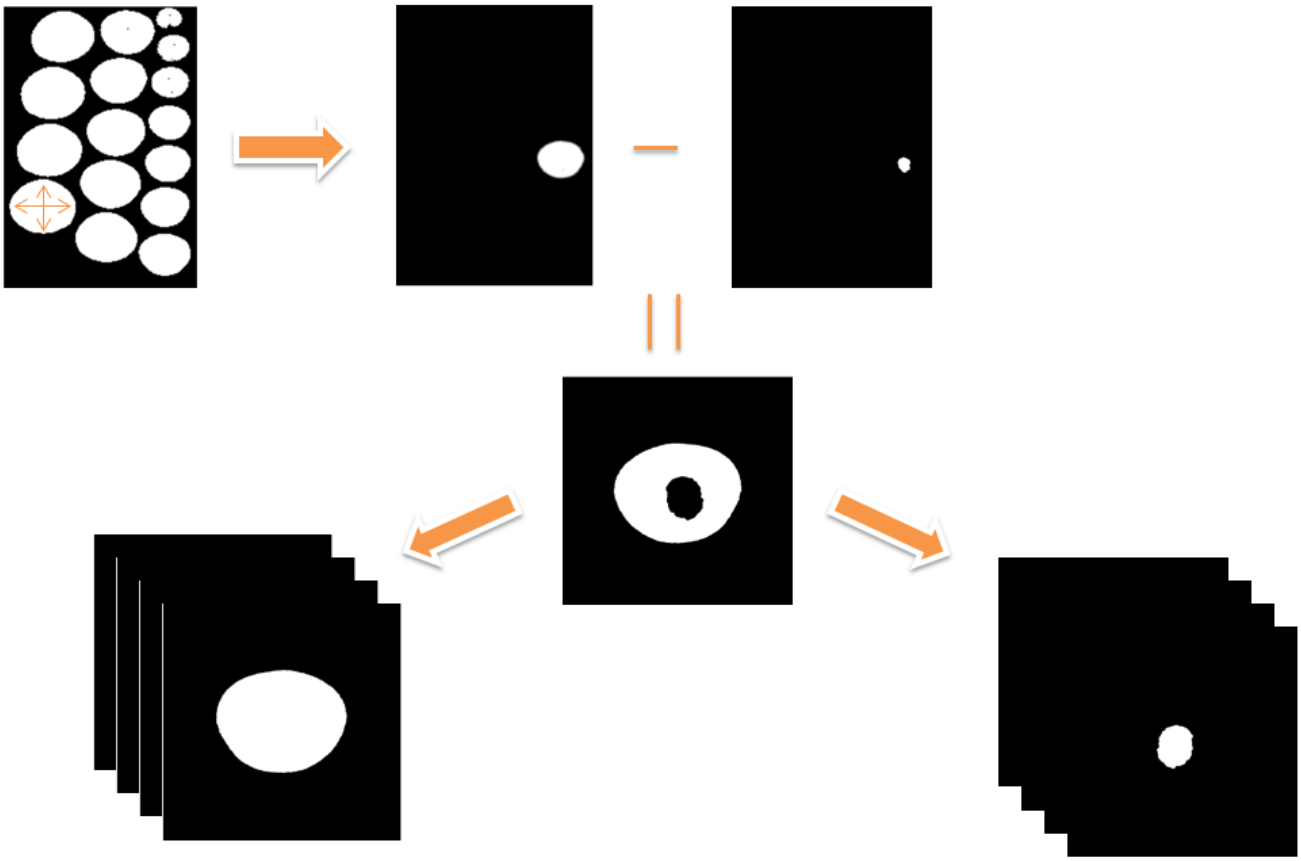

Figure 14: Schematic of how to obtain the stacks.

Those stacks were then aligned by means of affine transformations. Starting from the bottom slice each upper slice is aligned with respect to the lower.

3.3.3. Reconstruction

Then to reconstruct the potato volume it was necessary to thicken the slices using the mean width slice, and also calculate intermediate slices since the z resolution determined by the width of the slices is lower than the x,y resolution given by the scan.

To do that we discretized the boundary of the slices in a variable number of points dependent of how complicated was its boundary. Then, again starting from the bottom, we took the upper slice and compared the number of points of each one; the one with more required points to discretize its boundary is took as reference. Then for each point of the reference slice the nearest point of the other slice is founded. Once every point of the reference slice is paired with his nearest point of the pair slice a line between them is calculated and discretized into the desired number of intermediate slices. Thus we obtain a binary volumetric 3D image.

Then from the volumetric 3D image an isosurface is calculated, and there the vertices of the isosurface are scaled. The z component is scaled using the mean width slice, and the x and y components are scaled using the dpi (density pixels per inch) and the inch to cm factor conversion. Thus, the final isosurface has scaled to cm.

To obtain a mesh from this isosurface the iso2mesh library [Fang, Q., & Boas, D. A. (2009)] was used.

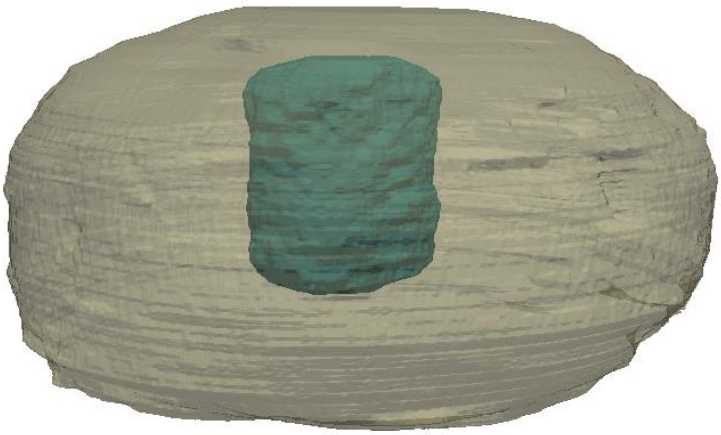

Figure 135: 3D reconstruction of a potato and its electroporated zone.

3.4. Numerical Simulations

3.4.1. Conductivity Curve Determination

To determine the conductivity curve of our potato variety we followed the work done in [10]. We used potato tubers, all of them with more or less the same size, and applied single pulses of

400us in a range between 0 to 600 V/cm. At the same time the pulses were registered with an oscilloscope and the data of voltage and current was stored.

The data was loaded and processed with MATLAB. From the current and voltage data we were able to calculate the conductivity of the sample at a given time during the pulse. In our case as did in [10] we analyzed the conductivity of the samples at 100 us.

To obtain the conductivity first we calculated the impedance of the sample. Using Ohm's law, the voltage value was obtained directly form the oscilloscope registers, and the current data was obtained dividing the registers of its particular channel in the oscilloscope by the value of the sensing resistance, which was 10 ohms in our case.

$$Z = \frac{V}{I}$$

Equation 1: Ohm's law

We assumed Z = R since the pulses were delivered as DC currents. The resistance of the potato tubers can be modelled as the resistance of wires of wide cross sectional areas. Then using equation 2, where L is the length of the potato tubers, A its cross sectional area and ρ the resistivity of the tubers, and knowing that conductivity is the inverse of the resistivity, the equation can be rearranged to obtain conductivity.

$$R = \frac{\rho L}{A}$$

Equation 2: Resistance of a wire

All potato tubers had the same cross sectional area which was 2.40cm^2 and the length was measured experimentally with the caliper at the same time as the electric pulses were delivered.

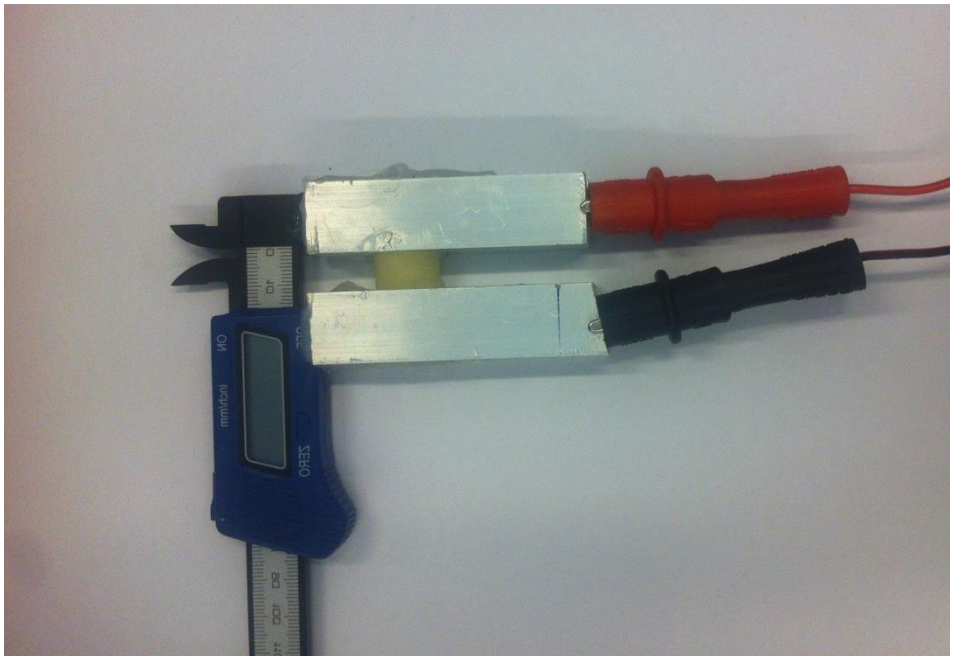

Figure 16: Caliper used to measure height of potato tubers and also their parallel plates act as electrodes.

Since the electrodes of the caliper are made of two parallel plates is possible to obtain the electrical field applied over potato tubers. As can be seen in Figure 17.

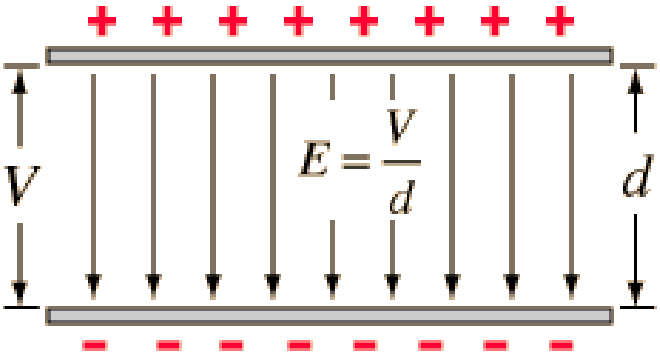

Figure 147: Electric field between parallel plates.

With the conductivity and electric field values obtained we were able to fit a sigmoidal function able to predict the conductivity of our potato type in function of the applied electric field.

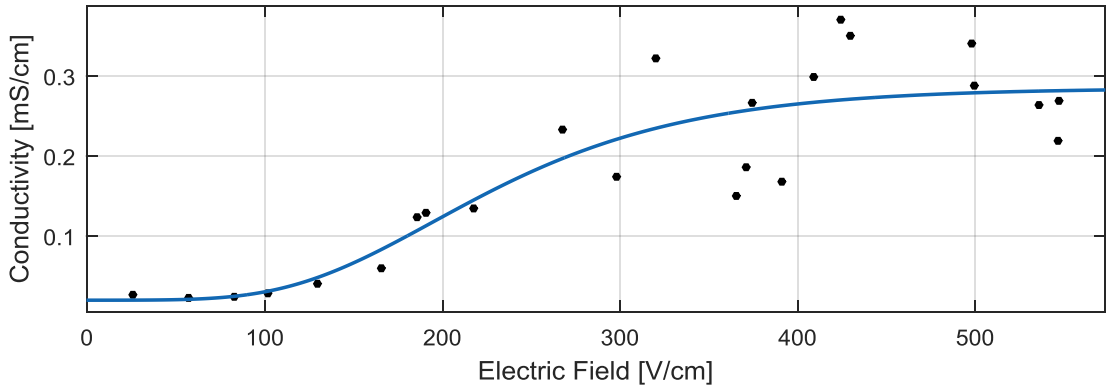

Figure 18: Experimentally determined conductivity function.

The upper sigmoidal curve can be fitted with the expression:

$$\sigma(|E|) = 0.01994 + 0.2651e^{-e^{-(0.01242(|E|-194.5))}} \left[\frac{mS}{cm}\right]$$

Equation 3: Conductivity function.

This function is the conductivity function which was used in all our FEM simulations.

3.4.2. Simulations of two needle electrode configuration

Finite element software (COMSOL Multiphysics) was used to calculate the electric field distributions within the tissue during IRE pulses. The 3D geometry used consisted on a sphere of 60 mm of diameter with two cylinders inserted separated 15 mm. These cylinders have 1.27 mm of diameter and 15 mm of length. In order to represent the isolator, two additional cylinders with 2 mm of diameter were placed.

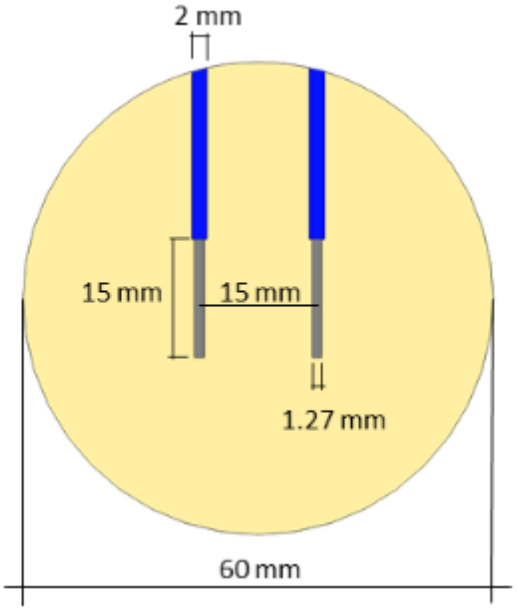

Figure 19: Schematic representation of the geometry used for mathematical models.

Isolation boundary condition was stablished in all boundaries except on the interface between active electrodes and tissue. In this case one of the electrodes surface was defined as a ground and the other one had fixed at simulated voltage.

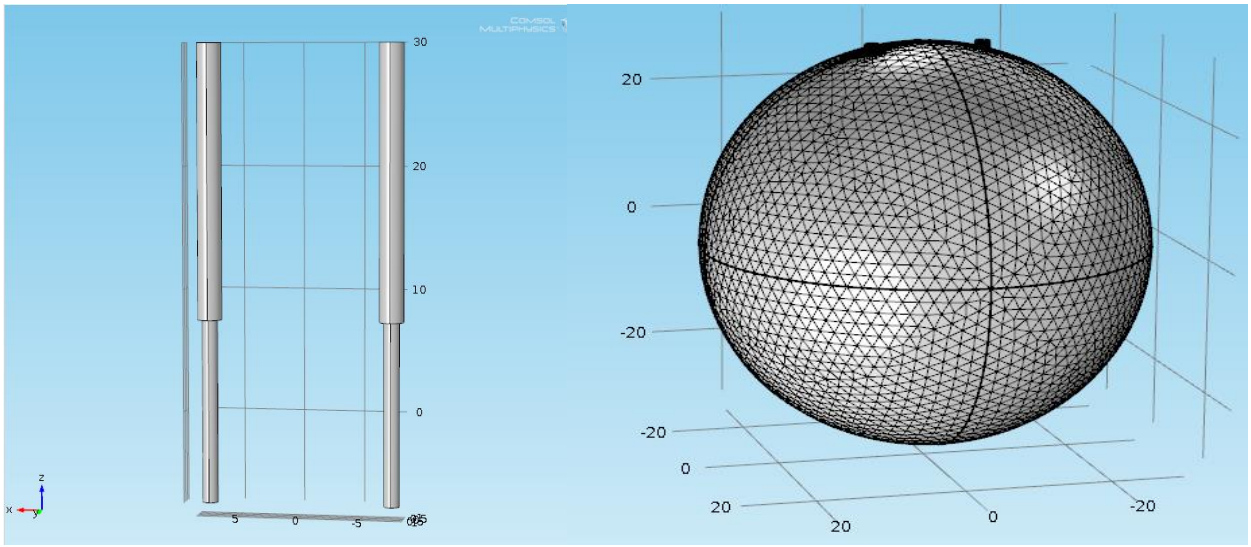

Figure 20: Electrodes geometry and sphere mesh used in FEM simulations.

Electric field distributions were stationary simulated with applied voltages between electrodes whose goes from 0 to 1250 V in steps of 50 V. The simulated volumes of electroporated tissue were calculated according to a threshold value of 161 [V/cm]. This threshold was obtained comparing the available experimental results with the simulations. Linear regression was used to fit the best threshold value.

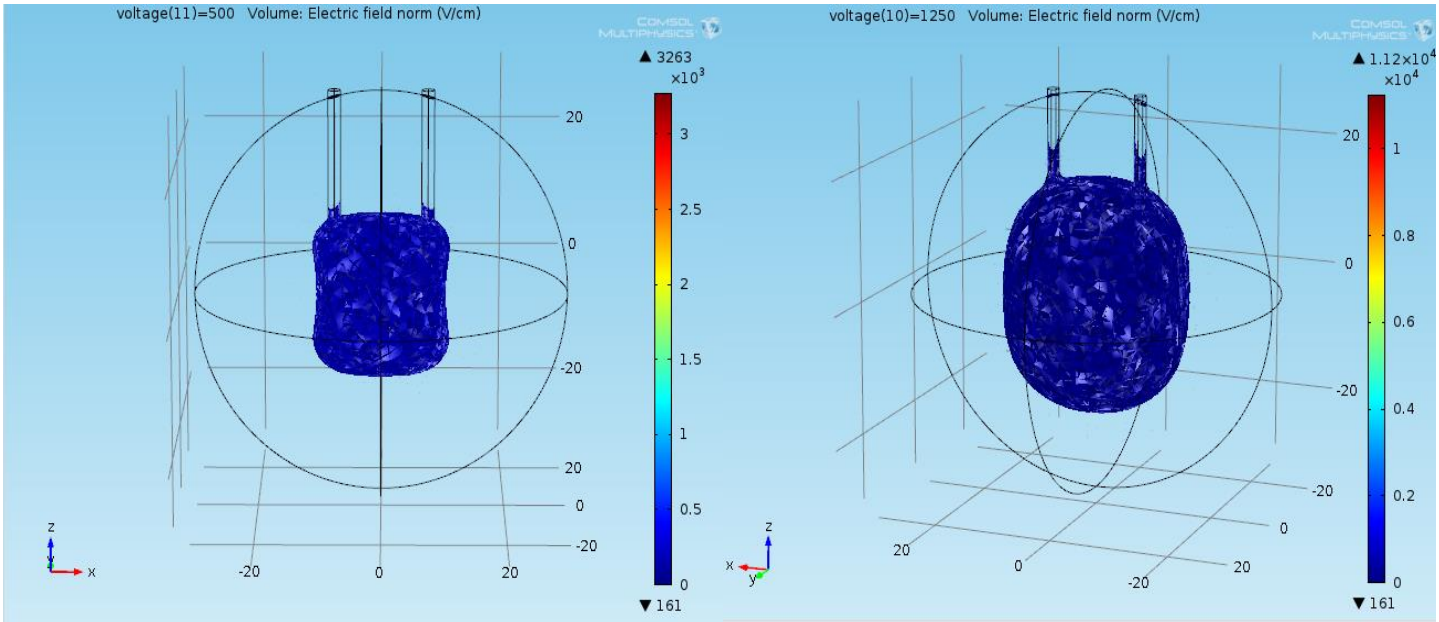

Figure 21: Simulated volumes of electroporated tissue using the experimentally determined threshold. On the left a simulation of 500V, on the right a simulation of 1250V.

4. Results

4.1. Osmolarity results

We found that the minimum difference between the area of the slices before and after the bath was produced with a solution of 0.9% of NaCl for the dye solution as can be seen in figure 22.

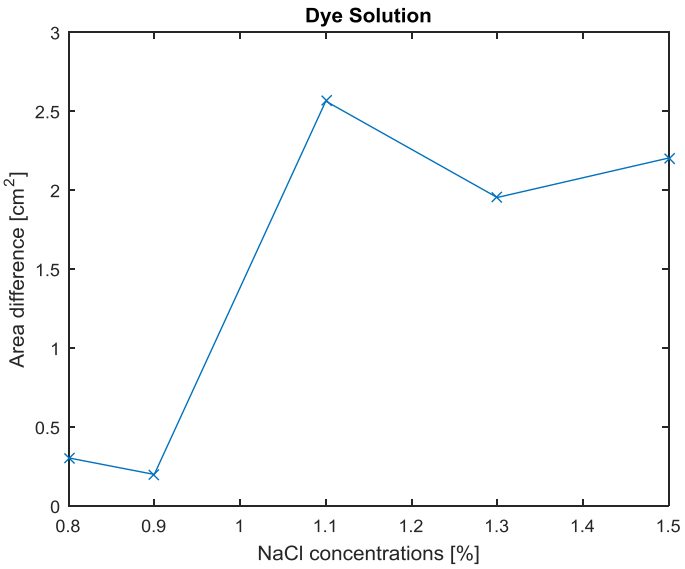

Figure 152: Osmolarity assessment for Dye Solution.

For the distilled water solution the minimum difference was found at 1.4% of NaCl. As can be seen in figure 23.

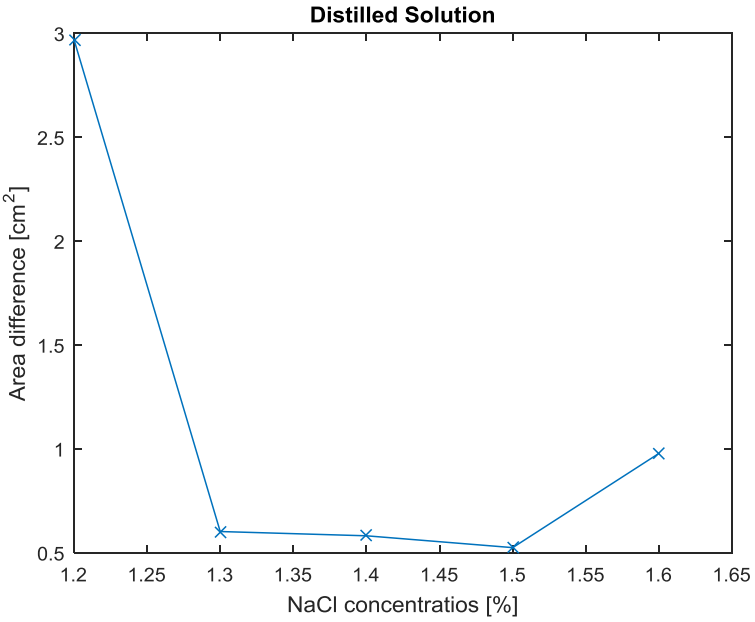

Figure 23: Osmolaity assessment for Distilled solution.

4.2. Voltage

Both simulated, dotted line, and experimental volumes under the effect of IRE increase lineally with the voltage. Also an increase of variability is observed in IRE volumes as voltage increase.

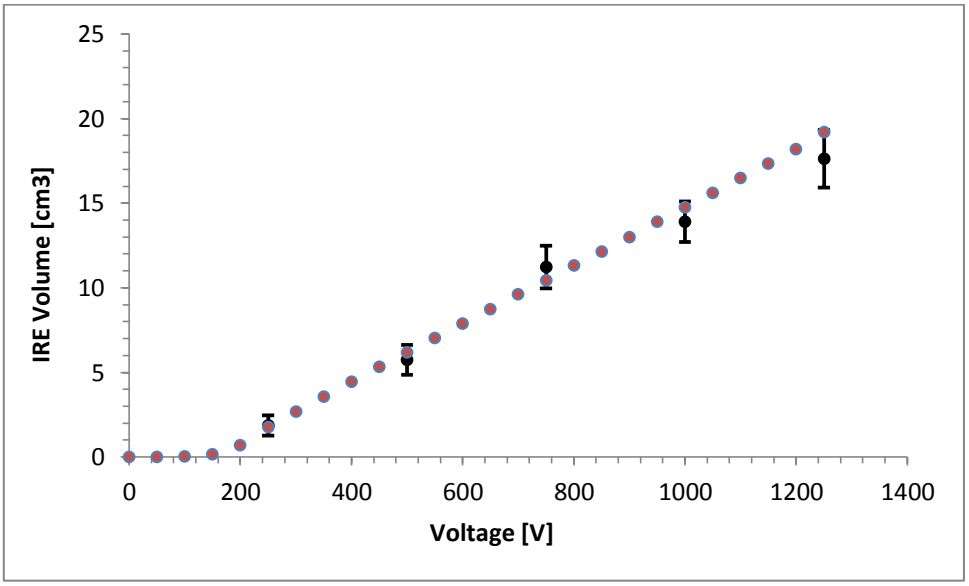

Figure 24: Voltage assessment

4.3. Number of pulses

As we increase the number of pulses the variability seems slightly to decrease and also a logarithmic behavior is observed,

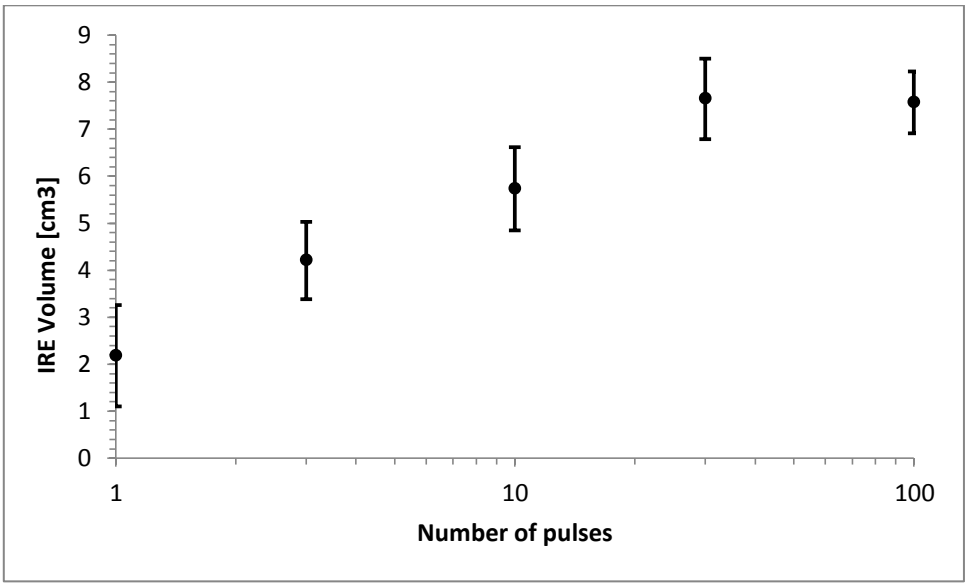

Figure 25: Number of pulses assessment

4.4. Pulse duration

We can see that as we increase the pulse duration the amount of affected volume increase lineally and the variability is reduced.

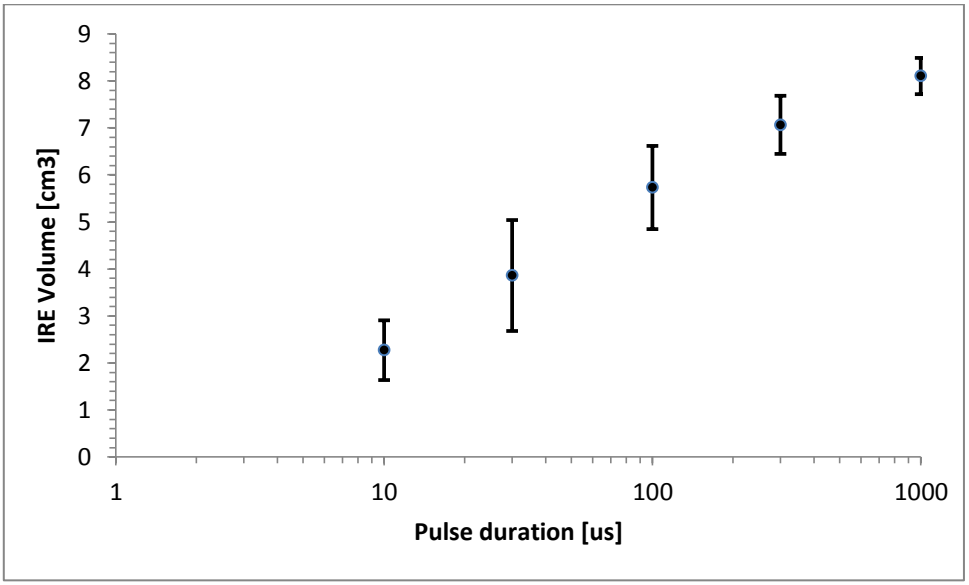

Figure 26: Duration of pulses assessment

5. Discussion and conclusions

The correlation results obtained between the simulations and the dyed area in figure 24 pointed out that dyed areas are the real electroporated areas, so the dye works properly as [24] suggested in their work.

The results in figure 24 and 26 agrees to the behavior reported in other studies which confirms the goodness of the experimental observations [21]. However the results of figure 25 suggest a new behavior that have to be took into account in future simulations.

It requires a certain amount of cumulative pulse time to achieve complete cell death even when above threshold electric field level. This can be achieved by either increasing the pulse duration or the total pulse number. This may explain the decrease of variability produced in both cases and also the increase in the voltage assessment. However, there are constraints on increasing pulse duration due to Joule heating, and procedure time is lengthened by increasing pulse number. [2]

We presented a new method for three-dimensionally asses the IRE outcomes using vegetal model. This method has been experimentally evaluated assessing the IRE treated volumes once different electric protocols were delivered. The observed values come close the theoretical predictions obtained by means of numerical simulations. It confirms the reliability of the presented evaluation method. This news assessment tool can be useful to improve both applied

protocols and prediction methods, thus, contribute to improve the clinical IRE treatment outcomes.

This project has given rise to a conference paper in the first world congress of electroporation (1st-WC-EP 2015).

6. Bibliography

[1] B. Rubinsky, G. Onik, and P. Mikus, “Irreversible electroporation: a new ablation modality--clinical implications.,” *Technol. Cancer Res. Treat.*, vol. 6, no. 1, pp. 37–48, 2007.

[2] C. Jiang, R. V Davalos, and J. C. Bischof, “A Review of Basic to Clinical Studies of Irreversible Electroporation Therapy,” vol. 62, no. 1, pp. 4–20, 2015.

[3] E. W. Lee, D. Wong, S. V. Prikhodko, A. Perez, C. Tran, C. T. Loh, and S. T. Kee, “Electron microscopic demonstration and evaluation of irreversible electroporation-induced nanopores on hepatocyte membranes,” *J. Vasc. Interv. Radiol.*, vol. 23, no. 1, pp. 107–113, 2012.

[4] M. L. Yarmush, A. Golberg, G. Serša, T. Kotnik, and D. Miklavčič, “Electroporation-Based Technologies for Medicine: Principles, Applications, and Challenges,” *Annu. Rev. Biomed. Eng.*, vol. 16, no. 1, pp. 295–320, 2014.

[5] R. E. Neal, P. A. Garcia, H. Kavnoudias, F. Rosenfeldt, C. A. Mclean, V. Earl, J. Bergman, R. V Davalos, and K. R. Thomson, “In Vivo Irreversible Electroporation Kidney Ablation : Experimentally Correlated Numerical Models,” vol. 62, no. 2, pp. 561–569, 2015.

[6] L. Towhidi, T. Kotnik, G. Pucihar, S. M. P. Firoozabadi, H. Mozdarani, and D. Miklavcic, “Variability of the minimal transmembrane voltage resulting in detectable membrane electroporation.,” *Electromagn. Biol. Med.*, vol. 27, no. 4, pp. 372–385, 2008.

[7] M. Pavlin, N. Pavšelj, and D. Miklavčič, “Dependence of induced transmembrane potential on cell density, arrangement, and cell position inside a cell system,” *IEEE Trans. Biomed. Eng.*, vol. 49, no. 6, pp. 605–612, 2002.

[8] T. Kotnik and D. Miklavc, “Electroporation for Electrochemotherapy and Gene Therapy,” in *Bioelectromagnetic Medicine*, M. MS, Ed. 2004, pp. 637–656.

[9] D. Miklavcic and L. Towhidi, “Numerical study of the electroporation pulse shape effect on molecular uptake of biological cells,” *Radiol. Oncol.*, vol. 44, no. 1, pp. 34–41, 2010.

[10] A. Ivorra, L. M. Mir, and B. Rubinsky, “Electric field redistribution due to conductivity changes during tissue electroporation: Experiments with a simple vegetal model,” in *IFMBE Proceedings*, 2009, vol. 25, no. 13, pp. 59–62.

[11] D. Miklavcic, M. Snoj, A. Zupanic, B. Kos, M. Cemazar, M. Kropivnik, M. Bracko, T. Pecnik, E. Gadzijev, and G. Sersa, “Towards treatment planning and treatment of deep-seated solid tumors by electrochemotherapy.,” *Biomed. Eng. Online*, vol. 9, p. 10, 2010.

[12] B. Kos, A. Zupanic, T. Kotnik, M. Snoj, G. Sersa, and D. Miklavcic, “Robustness of treatment planning for electrochemotherapy of deep-seated tumors,” *J. Membr. Biol.*, vol. 236, no. 1, pp. 147–153, 2010.

[13] Y. Granot, A. Ivorra, E. Maor, and B. Rubinsky, “In vivo imaging of irreversible electroporation by means of electrical impedance tomography.,” *Phys. Med. Biol.*, vol. 54, no. 16, pp. 4927–4943, 2009.

[14] E. W. Lee, C. T. Loh, and S. T. Kee, “Imaging guided percutaneous irreversible electroporation: ultrasound and immunohistological correlation.,” *Technol. Cancer Res. Treat.*, vol. 6, no. 4, pp. 287–294, 2007.

[15] C. Bertacchini, P. M. Margotti, E. Bergamini, A. Lodi, M. Ronchetti, and R. Cadossi, “Design of an irreversible electroporation system for clinical use.,” *Technol. Cancer Res. Treat.*, vol. 6, no. 4, pp. 313–320, 2007.

[16] V. Kasivisvanathan, A. Thapar, Y. Oskrochi, J. Picard, and E. L. S. Leen, “Irreversible electroporation for focal ablation at the porta hepatis,” *Cardiovasc. Intervent. Radiol.*, vol. 35, no. 6, pp. 1531–1534, 2012.

[17] N. Jourabchi, K. Beroukhim, B. a. Tafti, S. T. Kee, and E. W. Lee, “Irreversible electroporation (NanoKnife) in cancer treatment,” *Gastrointest. Interv.*, vol. 3, no. 1, pp. 1–11, 2014.

[18] D. Miklavcic, D. Semrov, H. Mekid, and L. M. Mir, “In vivo electroporation threshold determination,” *Proc. 22nd Annu. Int. Conf. IEEE Eng. Med. Biol. Soc. (Cat. No.00CH37143)*, vol. 4, 2000.

[19] R. E. Neal, J. L. Millar, H. Kavnoudias, P. Royce, F. Rosenfeldt, A. Pham, R. Smith, R. V. Davalos, and K. R. Thomson, “In vivo characterization and numerical simulation of prostate properties for non-thermal irreversible electroporation ablation,” *Prostate*, vol. 74, no. 5, pp. 458–468, 2014.

[20] K. Kurata, S. Nomura, and H. Takamatsu, “Three-dimensional analysis of irreversible electroporation: Estimation of thermal and non-thermal damage,” *Int. J. Heat Mass Transf.*, vol. 72, pp. 66–74, 2014.

[21] C. Suárez, A. Soba, F. Maglietti, N. Olaiz, and G. Marshall, “The Role of Additional Pulses in Electropermeabilization Protocols,” *PLoS One*, vol. 9, no. 12, p. e113413, 2014.

[22] I. N. A. Ashie and B. K. Simpson, “Application of high hydrostatic pressure to control enzyme related fresh seafood texture deterioration,” *Food Research International*, vol. 29, no. 5–6. pp. 569–575, 1996.

[23] R. N. Pereira, F. G. Galindo, A. A. Vicente, and P. Dejmek, “Effects of pulsed electric field on the viscoelastic properties of potato tissue,” *Food Biophys.*, vol. 4, no. 3, pp. 229–239, 2009.

[24] A. Janositz, a. K. Noack, and D. Knorr, “Pulsed electric fields and their impact on the diffusion characteristics of potato slices,” *LWT - Food Sci. Technol.*, vol. 44, no. 9, pp. 1939–1945, 2011.

[25] R. Stampfli, “Reversible electrical breakdown of the excitable membrane of a Ranvier node,” *Acad. Bras. Cienc.*, vol. 30, pp. 57–63, 1958.

[26] S. A and W. Hamilton, “Effects of high electric fields on microorganismsI. Killing of bacteria and yeasts,” *Biochimica et Biophysica Acta (BBA) - General Subjects*, vol. 148, no. 3. pp. 781–788, 1967.

[27] W. Hamilton and A. Sale, “Effects of high electric fields on microorganismsII. Mechanism of action of the lethal effect,” *Biochimica et Biophysica Acta (BBA) - General Subjects*, vol. 148, no. 3. pp. 789–800, 1967.

[28] A. J. H. Sale and W. A. Hamilton, “Effects of high electric fields on micro-organisms,” *Biochimica et Biophysica Acta (BBA) - Biomembranes*, vol. 163, no. 1. pp. 37–43, 1968.

[29] E. Neumann, M. Schaefer-Ridder, Y. Wang, and P. H. Hofschneider, “Gene transfer into mouse lyoma cells by electroporation in high electric fields.,” *EMBO J.*, vol. 1, no. 7, pp. 841–845, 1982.

[30] A. I. Daud, R. C. DeConti, S. Andrews, P. Urbas, A. I. Riker, V. K. Sondak, P. N. Munster, D. M. Sullivan, K. E. Ugen, J. L. Messina, and R. Heller, “Phase I trial of interleukin-12 plasmid electroporation in patients with metastatic melanoma,” *J. Clin. Oncol.*, vol. 26, no. 36, pp. 5896–5903, 2008.

[31] L. M. Mir, S. Orlowski, J. Belehradek, and C. Paoletti, “Electrochemotherapy potentiation of antitumour effect of bleomycin by local electric pulses.,” *Eur. J. Cancer*, vol. 27, no. 1, pp. 68–72, 1991.

[32] M. Belehradek, C. Domenge, B. Luboinski, S. Orlowski, J. Belehradek, and L. M. Mir, “Electrochemotherapy, a new antitumor treatment: First clinical Phase I-II trial,” *Cancer*, vol. 72, no. 12, pp. 3694–3700, 1993.

[33] D. Miklavčič, B. Mali, B. Kos, R. Heller, and G. Serša, “Electrochemotherapy: from the drawing board into medical practice.,” *Biomed. Eng. Online*, vol. 13, no. 1, p. 29, 2014.

[34] R. V. Davalos, L. M. Mir, and B. Rubinsky, “Tissue ablation with irreversible electroporation,” *Ann. Biomed. Eng.*, vol. 33, no. 2, pp. 223–231, 2005.

[35] J. F. Edd, L. Horowitz, R. V. Davalos, L. M. Mir, and B. Rubinsky, “In vivo results of a new focal tissue ablation technique: Irreversible electroporation,” *IEEE Trans. Biomed. Eng.*, vol. 53, no. 7, pp. 1409–1415, 2006.

[36] M. Pech, A. Janitzky, J. J. Wendler, C. Strang, S. Blaschke, O. Dudeck, J. Ricke, and U. B. Liehr, “Irreversible electroporation of renal cell carcinoma: A first-in-man phase i clinical study,” *Cardiovasc. Intervent. Radiol.*, vol. 34, no. 1, pp. 132–138, 2011.

[37] J. F. Edd and R. V Davalos, “Mathematical modeling of irreversible electroporation for treatment planning.,” *Technol. Cancer Res. Treat.*, vol. 6, no. 4, pp. 275–286, 2007.

[38] T. Wimmer, G. Srimathveeravalli, N. Gutta, P. C. Ezell, S. Monette, M. Maybody, J. P. Erinjery, J. C. Durack, J. a. Coleman, and S. B. Solomon, “Planning Irreversible Electroporation in the Porcine Kidney: Are Numerical Simulations Reliable for Predicting Empiric Ablation Outcomes?,” *Cardiovasc. Intervent. Radiol.*, pp. 182–190, 2014.